Title of Grant / Cooperative Agreement:	An Algorithm to Determine the Spatial and Temporal Distributions of Sea-ice Leads in the Artic
Type of Report:	Summary of Research
Name of Principal Investigator:	Steven Ackerman
Period Covered by Report:	05/24/2014 - 05/23/2018
Name and Address of recipient's institution:	University of Wisconsin System 21 N Park Street Suite 6401; Madison, WI 53715-1218
NASA Grant / Cooperative Agreement Number:	NNX14AJ42G

Reference 2 CFR § 1800.908 or 14 CFR § 1260.28 Patent Rights *as applicable (abbreviated below)*
The recipient may use whatever format is convenient to disclose subject invention required in subparagraph (c)(1). NASA prefers that the recipient use either the electronic or paper version of NASA Form 1679, Disclosure of Invention and New Technology (Including Software), to disclose subject inventions. Both the electronic and paper version of the NASA Form 1679 may be accessed at the electronic New Technology Reporting Web site https://invention.nasa.gov.
A final new technology summary report listing all subject inventions (or a statement certifying there were none) for the entire award period; which report shall be submitted within 90 days after the end date for the period of performance within the designated system noted within the award document."

Have any Subject Inventions / New Technology Items resulted from work performed under this Grant / Cooperative Agreement?	No ◉	Yes ○
If yes a complete listing should be provided here: Details can be provided in the body of the Summary of Research report.		

Reference 2 CFR § 1800.907 or 14 CFR § 1260.27 Equipment and Other Property *as applicable* (abbreviated below)
A Final Inventory Report of Federally Owned Property, including equipment where title was taken by the Government, will be submitted by the Recipient no later than 60 days after the expiration date of the grant. Negative responses for Final Inventory Reports are required.

Is there any Federally Owned Property, either Government Furnished or Grantee Acquired, in the custody of the Recipient?	No ◉	Yes ○
If yes please attach a complete listing including information as set forth at § 1260.134(f)(1).		

Attach the Summary of Research text behind this cover sheet.

Reference 2 CFR § 1800.902 or 14 CFR § 1260.22 Technical publications and reports *as applicable* (abbreviated below)
Reports shall be in the English language, informal in nature, and ordinarily not exceed three pages (not counting bibliographies, abstracts, and lists of other media).

A Summary of Research (or Educational Activity Report in the case of Education Grants) is due within 90 days after the expiration date of the grant, regardless of whether or not support is continued under another grant. This report shall be a comprehensive summary of significant accomplishments during the duration of the grant.

An Algorithm to Determine the Spatial and Temporal Distributions of Sea Ice Leads in the Arctic

Grant number: NNX14AJ42G
Final Report

University of Wisconsin - Madison
Space Science and Engineering Center
Cooperative Institute for Meteorological Satellite Studies
1225 W. Dayton Street, Madison, WI

Investigators:

Steven A. Ackerman (PI)
Jay Hoffman
Jeffrey Key
Yinghui Liu

Table of Contents

Overview

The goal of this project is to develop an algorithm and an accompanying Algorithm Theoretical Basis Document (ATBD) to detect sea ice leads from the MODerate Resolution Imaging Spectrometer (MODIS) instruments on Terra and Aqua. The ATBD describes the algorithm and demonstrates applications. We were able to run the algorithm over the entire MODIS Aqua/Terra period (2003-2018) for the months of January-April and produce the data on our local computer resources.

1. Introduction

Leads are elongated cracks in the sea ice cover. They form under stresses due to atmospheric winds and ocean currents (e.g., Smith et al., 1990). The open water refreezes as it is exposed to a cold atmosphere, so leads may contain unfrozen water or ice of varying thicknesses. They may be a few meters or a few kilometers in width, and may be tens of kilometers in length. In comparison to ice-covered regions, leads provide a significant amount of heat and moisture to the Arctic atmosphere (e.g. Alam and Curry 1995, Maykut, 1987). While leads may occupy a relatively small area of pack ice (e.g. 1-2% of an area), the open waters provide a significant exchange of heat and moisture between the ocean and atmosphere, particularly during winter. They are also important for navigation and wildlife.

One of NASA's science objectives is to address the question: "*How and why are Earth's climate and the environment changing*?" This project addresses this question by characterizing the distribution of leads in the Arctic Ocean. Observations of sea ice lead characteristics need to be measured to understand changes in the sea-ice and their response to atmospheric and oceanic forcing. Understanding these responses should ultimately enable more accurate climate predictions and characterizations of uncertainties. Recent observed declines in ice extent and area result from a warming of the atmosphere and ocean, which drives a decrease in ice thickness and perhaps an expansion of leads, even though there might be more ice production during winter as ice reforms in the leads. To fully understand this dynamic between the Arctic sea ice area and thickness, the area coverage of leads and atmosphere and ocean circulations, we need to measure the general distribution of leads and determine how this distribution has been changing. We begin this understanding with the development of an algorithm to achieve those measurements.

2. Accomplishments

Our initial approach relied on the Key et al. (1993 and 1994) algorithm. Those studies applied the algorithm to locate leads then determine their length, width and orientation. While

developed for LandSat, which has limited coverage of the polar ice caps, the methodology is portable to other optical sensors, such as AVHRR and the NASA MODIS imagers. AVHRR and MODIS have better spatial coverage and temporal coverage, but lack the spatial resolution of LandSat. Key et al. (1993) explored the sensitivity to lead detection using the AVHRR thermal imagery under various atmospheric conditions. Their results indicated that the limits of lead detection could be determined as a function of subpixel lead fraction and atmospheric optical depth, if suitable values of normalized contrast were used in the detection criteria.

Over the course of this project we developed a sea ice leads detection and characterization algorithm to run on MODIS data, wrote an ATBD, and applied the algorithm to the MODIS Terra/Aqua period. The technical overview of the approach requires the following steps:

- Access MODIS granules
- Stitch together the granules in an orbit that covers the arctic region
- Determine the fraction of cloud cover (from MOD35 and MYD35)
- Determine the fraction of ice coverage in a pixel
- Identify potential lead objects where the ice fraction within the pixel is less than 95%
- Connect objects that are close (within a couple of pixels)
- Identify linear features using imaging analysis tools, such as Hough transform, Sobel filtering and connectivity.
- Determine lead properties (length, area, etc.)

The flow chart of the algorithm is shown in Figure 1. Appendix A is the original ATBD that describes the algorithm in detail.

The list of conference presentations is below and we are ready to submit a paper on the algorithm for peer review. A paper for submission to a peer reviewed journal is near completion.

Algorithm Application

The algorithm was applied to Aqua and Terra MODIS observations between 2004 and 2018 for the months of January through April. We are using this time to identify trends that may reflect issues or errors with the algorithm. An animation of the analysis can be found here: https://www.ssec.wisc.edu/leads/results/.

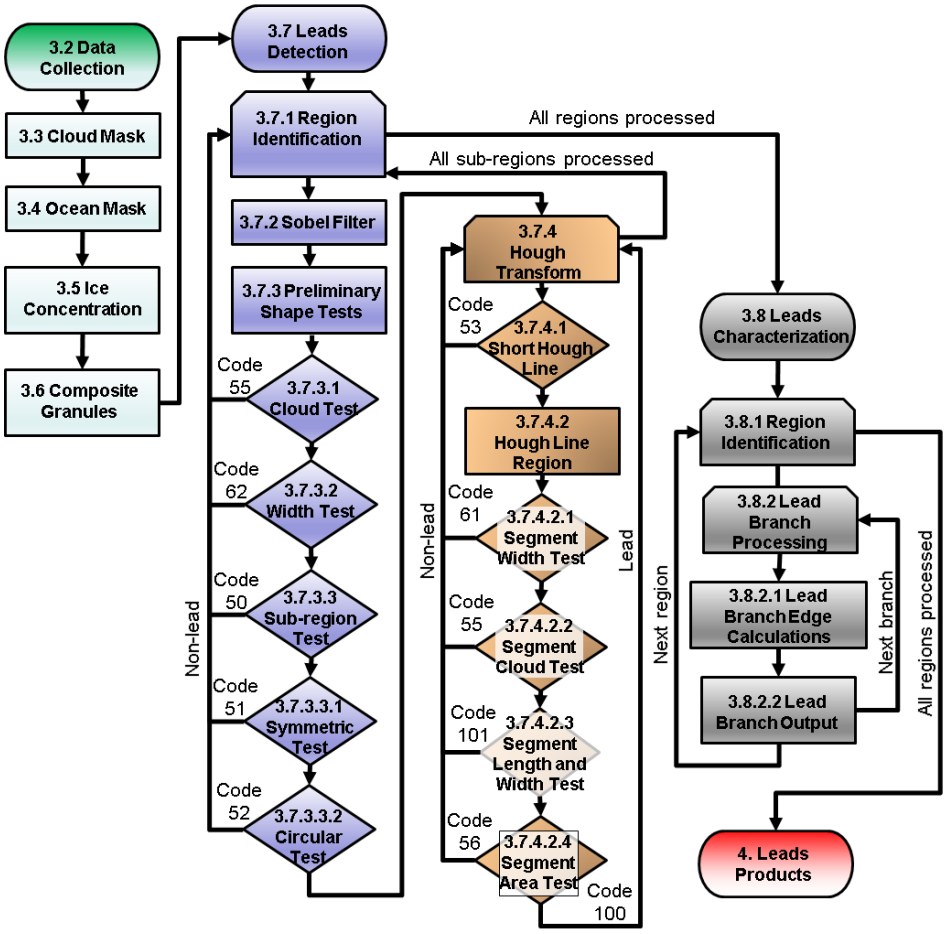

Figure 1 Leads algorithm flowchart.

Next Steps

The resources at SSEC are capable of executing the algorithm and producing a data set. We will make the data available from our web page (https://www.ssec.wisc.edu/leads/). In addition, we want to have the data in an appropriate Distributed Active Archive Centers (DAAC). We have begun discussion with Miguel O. Román, Terra/Aqua/Suomi-NPP Land Discipline Group Lead, on the best DAAC to archive the data. Since we can produce the data product on site, we don't require the Land SIPS, which processes cryosphere products, but do require a review of the ATBD. Following the Land/Cryo group practice, the detailed ATBD in Appendix A is being written as a peer review paper and will be submitted to a journal with an impact factor greater than 1.45. The paper will follow the same style/format as the Land/Cryo ATBD outline (https://viirsland.gsfc.nasa.gov/PDF/ATBD_Outline_Land.pdf). Once accepted the word version of the paper can be submitted as the NASA ATBD.

4. Conference Presentations

Ackerman, S. A., J. P. Hoffman, J. R. Key, Y. Liu, 2018: Arctic Sea Ice Leads from MODIS/VIIRS Observations. EUMETSAT Annual meeting, Tellin, Estonia, September 17-21.

Hoffman, J. P., S. A. Ackerman, Y. Liu, and J. R. Key, 2017: Satellite Detection of Arctic Sea Ice Leads, 2017: 97th Annual meeting of the American Meteorological Society, Seattle, WA, January 22 - 26

Hoffman, J., S. A Ackerman, Y. Liu, J. R. Key, 2016: Trends in Arctic Sea Ice Leads Detection. American Geophysical Union Fall meeting, San Francisco CA, December 12-16.

Hoffman, J. P., S. Ackerman, Y. Liu, and J. Key, 2016: Characterizing Arctic Sea Ice Leads from Space. 21st AMS Satellite Meteorology and Oceanography Conference, Madison WI, Aug 15-19

Ackerman, S. A., J. P. Hoffman, J. R. Key and Y. Liu, 2015: MODIS observations of the spatial and temporal distributions of sea-ice leads in the Arctic. EUMETSAT Annual meeting, Toulouse, FR, 21-25 September.

5. References and Citations

Alam, A. and J. Curry, 1995: Lead-induced atmospheric circulations. *Jour Geo Res*, **100**, C3, 4643-4651.

Key, J., J.A. Maslanik, and E. Ellefsen, 1994: The effects of sensor field-of-view on the geometrical characteristics of sea ice leads and implications for large-area heat flux estimates. *Remote Sensing Environ*., **48**(3), 347-357.

Key, J., R. Stone, J. Maslanik, and E. Ellefsen, 1993: The detectability of sea ice leads in satellite data as a function of atmospheric conditions and measurement scale. *Annals Glaciol*., **17**, 227-232.

Maykut, G. A., 1978: Energy exchange over young sea ice in the central Arctic. *J. Geophys. Res*., **83** (C7), 3646-3658.

Smith, S. D., R. D. Muench and C. H. Pease, 1990: Polynyas and leads: An overview of physical processes and environment, J. *Geophys. Res*. **95**, 9461-9470.

APPENDIX A: Algorithm Theoretical Basis Document

Algorithm Theoretical Basis Document

Sea-ice Leads in the Arctic

Jay Hoffman[1], Steven A. Ackerman[1], Yinghui Liu[1], Jeffrey Key[2]

[1]Cooperative Institute for Meteorological Satellite Studies, University of Wisconsin-Madison

NOAA/NESDIS, Madison, WI

Version 1.0

13 July 2018

Table of Contents

LIST OF FIGURES

LIST OF TABLES

ABSTRACT

This document presents a new methodology to detect and characterize sea ice leads with infrared satellite data. Leads are fractures in the ice cover that may be new and unfrozen or covered with thin ice. They play a critical role in the exchange of mass and energy between the ocean and atmosphere in the polar regions, particularly in the Arctic. Using the 11 μm brightness temperature, this algorithm derives thermal contrast in cloud-free regions and creates a mask of potential lead pixels. This algorithm identifies and characterizes leads with a combination of image processing techniques that examine shape characteristics. We use data from the Moderate Resolution Imaging Spectroradiometer (MODIS) to assess the spatial and temporal distributions of Arctic sea ice leads and their changes from 2003 to 2018. A new product can be used to identify lead characteristics (width, orientation, and spatial distribution), and their trends. From an operational perspective, knowledge of lead characteristics can aid in navigation, with direct benefits to security, subsistence hunting, and recreation.

1. Introduction

Leads are elongated fractures (cracks) in the sea ice cover. They form under stresses due to atmospheric winds and ocean currents (Smith et al., 1990). The open water refreezes as it is exposed to a cold atmosphere, so leads may contain unfrozen water or ice of varying thicknesses. They may be a few meters or a few kilometers in width and may be tens of kilometers in length. In comparison to ice-covered regions, leads provide a significant amount of heat and moisture to the Arctic atmosphere (Alam and Curry 1995; Maykut, 1987). While leads may occupy a relatively small area of pack ice (e.g. 1-2% of an area), the open waters provide a significant source of heat and moisture to the atmosphere, particularly during winter. They are also important for navigation and wildlife.

The long-term distribution of leads in sea ice and how these distributions might be changing is not well known. With the rapid thinning of the ice pack over the last few decades, along with the reduction in sea ice area and the recent increase in sea ice velocity (Hakkinen et al., 2008), we hypothesize that we will see a change in the lead distributions and properties from earlier studies, and likely in the time period of MODIS since 2003. Knowledge of this distribution of leads is important of climate and energy budget studies of the Arctic region.

Recent satellite observations show dramatic changes in the Arctic sea ice, including a trend of shrinking sea ice extent and area over the last decade and a thinning of the sea ice. The ICESat and future ICESat-2 NASA missions contribute to these finding. The ICESat missions seek to determine inter-annual and long-term changes in polar ice-sheet volume to sufficient accuracy to assess their impact on global sea level (Zwally et al., 2002). The AMSR-E instrument on NASA's Aqua mission, and now AMSR2 on Japan's GCOM-W1 satellite, aid in the monitoring of

sea ice extent and motion. Categorizing leads, including area coverage, frequencies, length and orientation, will contribute to these missions in the study of Arctic sea ice.

Leads impact climate in a number of ways. Leads have a lower albedo than the surrounding ice, and thus absorb more solar energy than surrounding ice. An increase in the ice leads can warm water beneath the leads and increase the melting of the surround ice. When leads open, the warmer ocean water releases heat and moisture into the atmosphere and impact the atmospheric structure and cloud properties above. Comparison of results from this proposal with trends in other Arctic sea ice properties (e.g. thickness, coverage, movement) and in atmospheric parameters (e.g. wind speed and direction) will help understand the ice dynamics under changing environment conditions, and interactions of climate system components.

One of NASA's science objectives is to address the question: "How and why are Earth's climate and the environment changing?" This algorithm provides a data archive of Artic Ocean sea ice lead characteristics that can help answer this question. Observations of sea ice lead characteristics provide information on changes in the sea ice and their response to atmospheric and oceanic forcing. Understanding these responses should ultimately enable more accurate climate predictions and characterizations of uncertainties. Recent observed declines in ice extent and area result from a warming of the atmosphere and ocean, which drives a decrease in ice thickness and perhaps an expansion of leads, even though there might be more ice production during winter as ice reforms in the leads. To fully understand this dynamic between the Arctic sea ice area and thickness, the number and area coverage of leads and atmosphere and ocean circulations, we need to measure the general distribution of leads and determine how this distribution has been changing. We begin this with the development of an algorithm to achieve those measurements.

1.1. Purpose of This Document

This document provides a high-level description of the physical basis for detecting and estimating characteristics of sea ice leads using infrared satellite data. It describes the algorithm, demonstrates applications, and provides example data sets.

1.2. Who Should Use This Document

The intended users of this document are those interested in understanding the physical basis and technical implementation of this algorithm, and how to use the output of this algorithm for a particular application. This document also provides information for implementing, maintaining, and potentially improving the original algorithm.

1.3. Revision History

Version 1.0 is the first delivered version of the ATBD.

2. Instrument Description

The leads detection algorithm is applied to data from the Moderate Resolution Imaging Spectroradiometer (MODIS) on NASA's Terra and Aqua satellites. MODIS instrument has broad spectral range (36 bands between 0.415–14.235 μm), high spatial resolution (250 m for 5 bands, 500 m for 5 bands, and 1000 m for 29 bands), frequent observations of polar regions (28 times a day for Terra and Aqua satellites), and low thermal band instrument noise (roughly 0.1 K for a 300 K scene) (Ackerman et al. 1998). MODIS cloud mask are developed by Ackerman et al. (1998) and has been improved in the polar regions (Liu et al. 2004; Frey et al. 2008). The MODIS level-2 cloud mask (MOD35_L2 for Terra and MYD35_L2 for Aqua) provides cloud cover with four confidence levels: confident clear, probably clear, uncertain/probably cloudy, and cloudy. Clear sky in this algorithm includes MODIS pixels of confident-clear and probably-clear in MODIS level-2 cloud mask.

3. Algorithm Description

In the MODIS sea ice leads algorithm, thermal contrast is calculated and used to form a daily composite from which image analysis methods detect and then characterize leads. This section describes the algorithm in detail.

3.1. Algorithm History

Our initial approach relied on the Key et al. (1993, 1994) algorithm, which located lead pixels in a binary image, grew lead fragments from connected lead pixels, connected lead fragments into lead objects, then determined the widths and orientations of the objects through a regression analysis. While developed for LandSat, which has limited coverage of the polar ice caps, the methodology is portable to other optical sensors, such as AVHRR and the NASA MODIS imagers. AVHRR and MODIS have better spatial and temporal coverage but lack the spatial resolution of LandSat.

Key et al. (1993, 1994) and Key (1994) explored the sensitivity of lead detection to measurement scale (pixel size). It was found that measurement scale has a significant effect on derived lead width distributions, where leads smaller than 250 m disappear from the distribution when pixel size increases beyond 320 m. However, this depends strongly on the contrast between the lead and the surrounding ice. A large thermal contrast, as would be expected in the winter, maintains the detectability of the lead with larger pixel sizes, though its derived width may increase. Key et al. (1993) and Stone and Key (1993) took this further by demonstrating the complexity of lead detection when varying atmospheric conditions are combined with measurement scale. They quantified the "critical contrast" needed to detect leads as a function of the optical depths of aerosols, ice crystal precipitation, and cirrus cloud, in combination with varying pixel size.

3.2. Algorithm Overview

The Aqua and Terra MODIS granules of level-2 cloud mask and 11 μm brightness temperature north of 66.5N are collected and remapped to a 1 km grid, Equal-Area Scalable Earth Grid version 2 (EASE2-Grid), using a nearest neighbor approach. The leads detection algorithm next identifies cloud-free ice-covered pixels over ocean water. Cloud screening is done using the MODIS cloud mask (MxD35) (Ackerman et al. 1998; Frey et al. 2008). The algorithm performs a series of test on the 11 μm brightness temperature, described in further detail in Section 3.6.

A daily composite is defined in a 1 km grid to record the number of overpasses that pass the thermal tests. From the daily threshold count, leads are identified using a number of image processing techniques. Finally, leads characteristics are derived from the subset of locations that have passed the initial leads detection tests. Figure 1 is a flowchart that summarizes the algorithm.

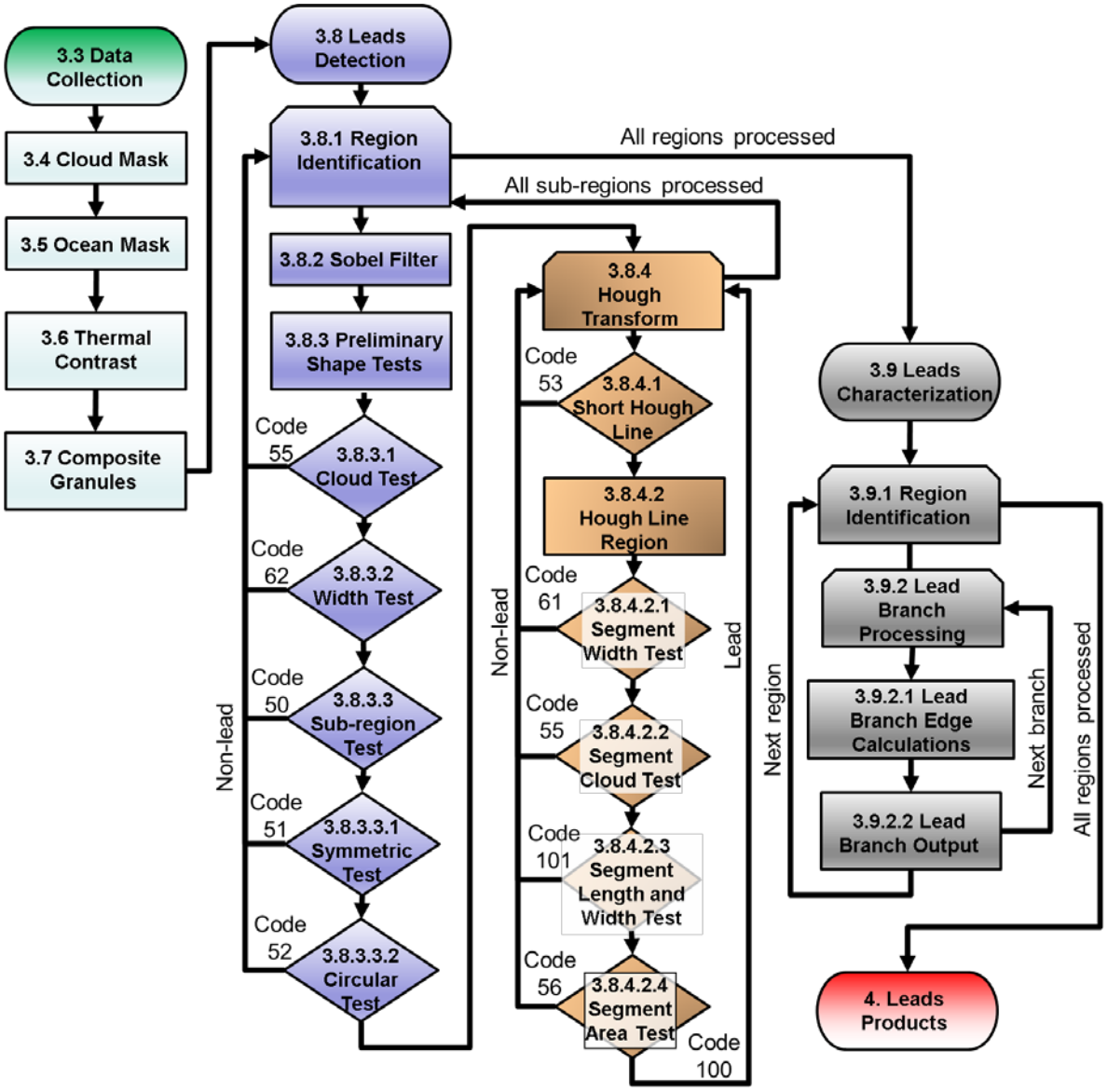

Figure 1. Leads algorithm flowchart. The numbers correspond to section numbers that further describe each step.

3.3. Data Collection

All Aqua and Terra level-2 overpasses are collected from January through April where at least half of the granule is north of 66.5^{o} latitude from the year of 2003 through 2018. The Level-1 11µm (band 31) brightness temperatures, cloud mask, and geolocation files were acquired from the Level-1 and Atmosphere Archive & Distribution System (LAADS) Distributed Active Archive

Center (DAAC), Located in the Goddard Space Flight Center in Greenbelt, Maryland (https://ladsweb.nascom.nasa.gov/).

3.4. Cloud Mask

Cloud screening is done using the cloud mask (MxD35) (Ackerman et al. 1998; Frey et al. 2008). When the solar zenith angle is less than 85 degrees, the unmodified cloud mask is used, elsewhere the mask is modified using a spatial filter to remove clouds for night-time overpasses (Fraser and Massom 2009). The cloud mask mean is calculated from a square window of a width of 5-pixels. When less than half of all the pixels in the window are clouds, the center pixel is re-classified as clear. An example cloud mask from 15 February 2018 at 0545 UTC is shown in Figure 2, where the cloud masked regions reclassified as clear by the spatial filter are highlighted in green, blue, and red; clear regions are black; and white flagged cloudy. A threshold of 50% was chosen (green and blue changed from cloudy to clear, red remains cloudy) in order to reduce most thin spatially features from the cloud mask while also preserving the cloud edges. This filter is important because several of the features flagged as clouds by the operational MODIS cloud mask at night appear to be leads. Only cloud pixels after the application of the spatial filter (white and red in Figure 2) are disqualified from lead detection. For reference, a map showing where this case is located in the Arctic is shown in Figure 3.

Figure 2. MODIS-TERRA cloud mask image from 15 February 2018, at 0545UTC. The original cloud mask defines clouds as all non-black areas; a spatial filter is applied to remove thin features from the mask. In green 25% or less of the local mean is cloudy, 50% or less of the local mean is cloudy in blue – these regions are removed from the night-time cloud mask. In red 75% or less of the local mean is cloudy – these regions remain classified as cloudy.

Figure 3. Map of region of interest used for case study example.

3.5. Ocean Mask

Lead detection are limited to oceans. Land and fresh-water area are eliminated from lead detection by this algorithm.

3.6. Thermal Contrast

There is relatively little thermal contrast across frozen water features (ice and ice-covered snow), whereas there often is a sharp contrast between frozen and open water. A pixel is identified as a possible lead if the brightness temperature is less than 271 K. The threshold of 271K was chosen because, as shown in Figure 4, warmer brightness temperatures are more likely to be rejected due to geometric testing. Brightness temperatures warmer than 271K tend to be contaminated by artifacts from (warm) cloud mask detection omission errors or else it may be open water without any nearby sea ice (not a lead). There is also a contrast test procedure similar to what Willmes and Heinemann (2015) describe as part of their algorithm. For each pixel, the mean and standard deviation of brightness temperature for a region of 25x25 pixels – centered on the point of interest - are calculated. To define a potential lead, a cloud-free, water pixels must have an 11 µm brightness temperature minus the mean brightness temperature greater than 1.5K and greater than the local window standard deviation. Our technique deviates from Willmes and Heinemann (2015) as we are using the 11 µm brightness temperature rather than the derived ice surface temperature product. Also, we constrain the MODIS scan angle to 30 degrees; beyond 30 degrees we do not attempt to retrieve leads due to the degradation of spatial resolution. An example 11 µm brightness temperature image is shown in Figure 5 and the corresponding pixels flagged as potential leads after thermal contrast test is shown in Figure 6.

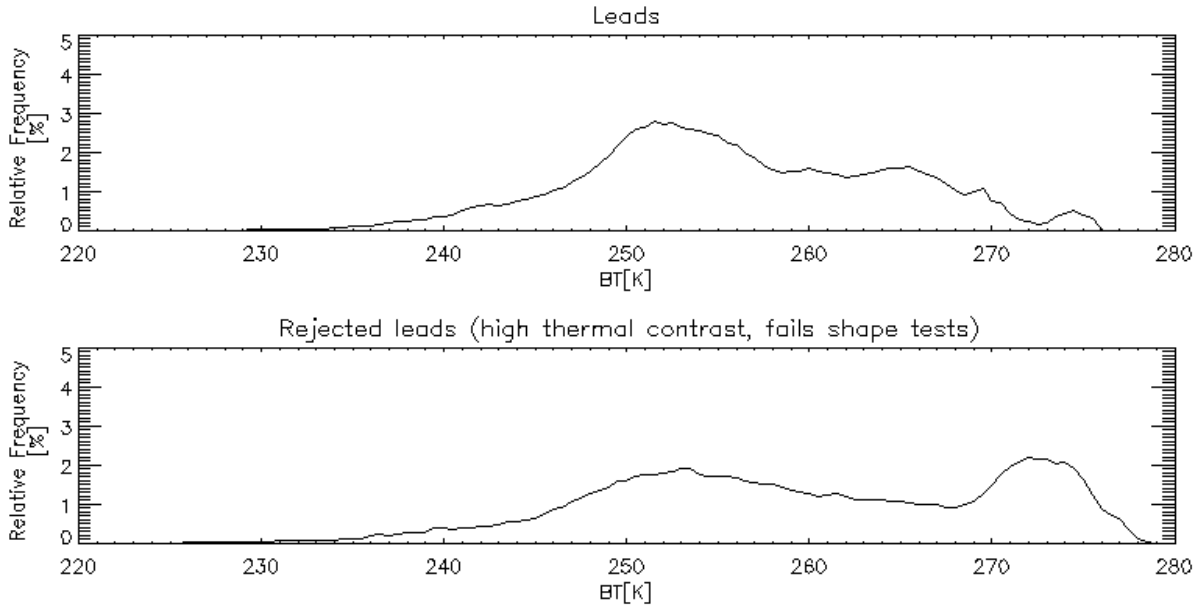

Figure 4. Histogram of 11µm brightness temperature where leads (top) and rejected leads (bottom) are found. For this example, no constant temperature is applied (only thermal contrast tests). Leads are identified only by thermal the local window mean and standard deviation tests; leads can be rejected due to geometric tests (described in Section 3.8).

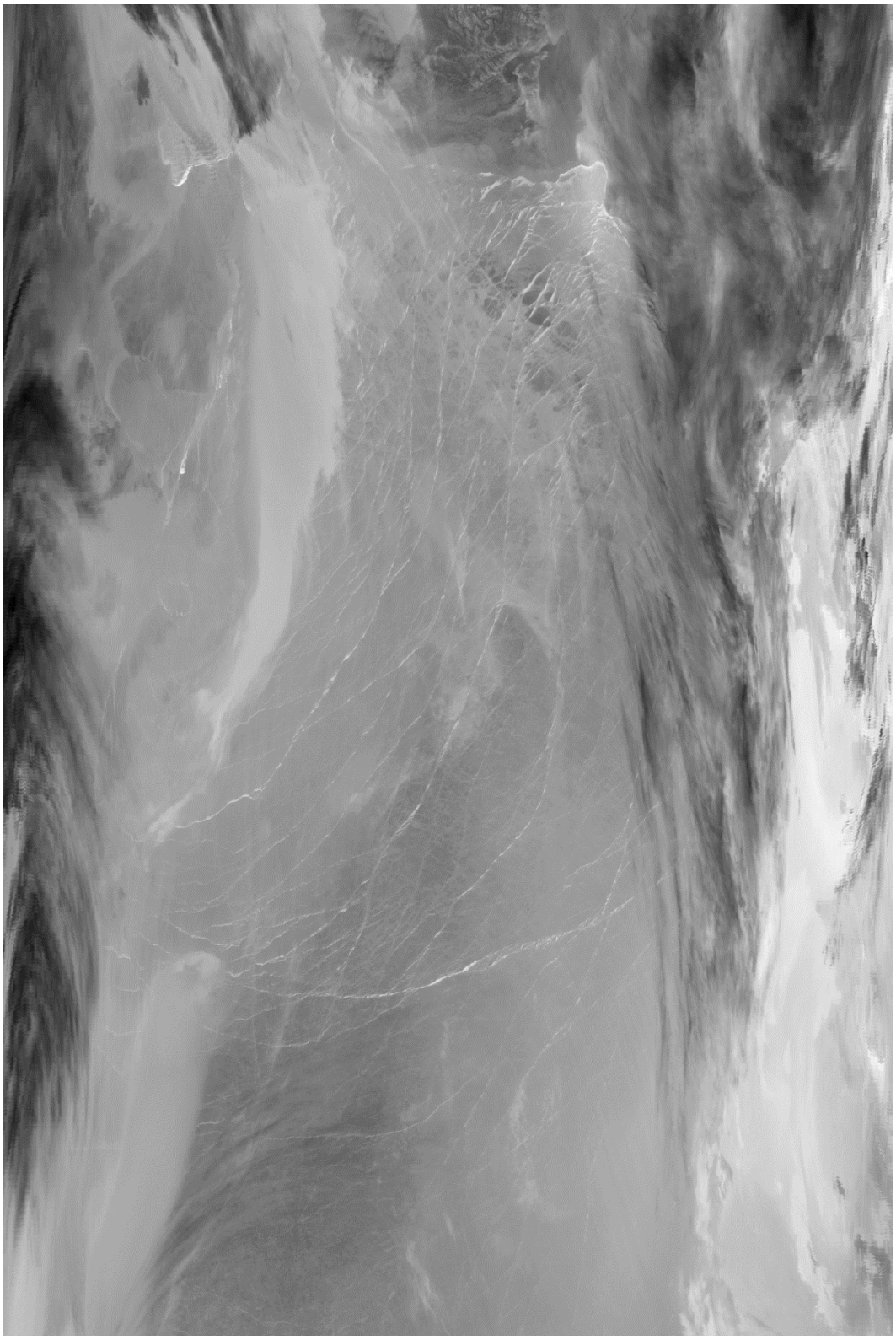

Figure 5. MODIS-TERRA BT31 image from 15 February 2018 at 0545UTC. Notice leads are readily apparent as bright (warm) features relative to the darker (colder) ice and clouds.

Figure 6. MODIS-TERRA potential lead mask from the case study overpass from 0545 UTC on 15 February, 2018. Potential leads are in black, clouds are white, land is brown and the scan angle block out is illustrated in red.

3.7. Compositing Granules

After running the thermal contrast technique for each MODIS overpass, a daily composite image is generated using a 1 km Equal-Area Scalable Earth Grid version 2 (EASE2-Grid). This composite mask is generated as a count of potential leads (the number of overpasses where thermal contrast detected a potential lead), an example is shown in Figure 7. In addition to the composite count, composites of the number of cloudy and total overpasses each location are generated – these counts will help in later steps to establish detection confidence. An example is shown in Figure 8, where the majority of the potential leads (from Figure 7) are found in regions with 6 or more clear overpasses (green).

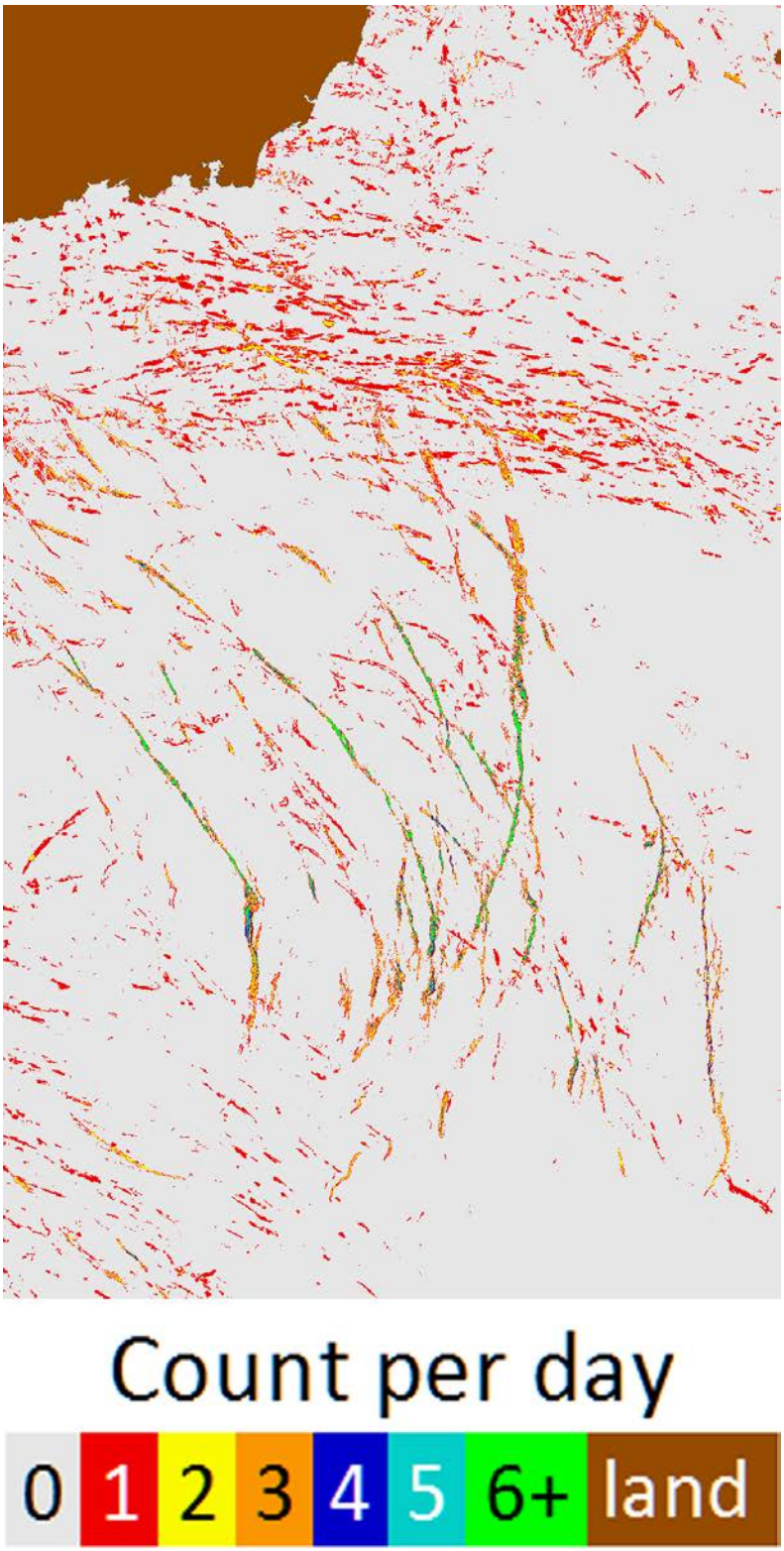

Figure 7: The number of overpasses when a potential lead is detected on 15 February 2018 in the Beaufort Sea.

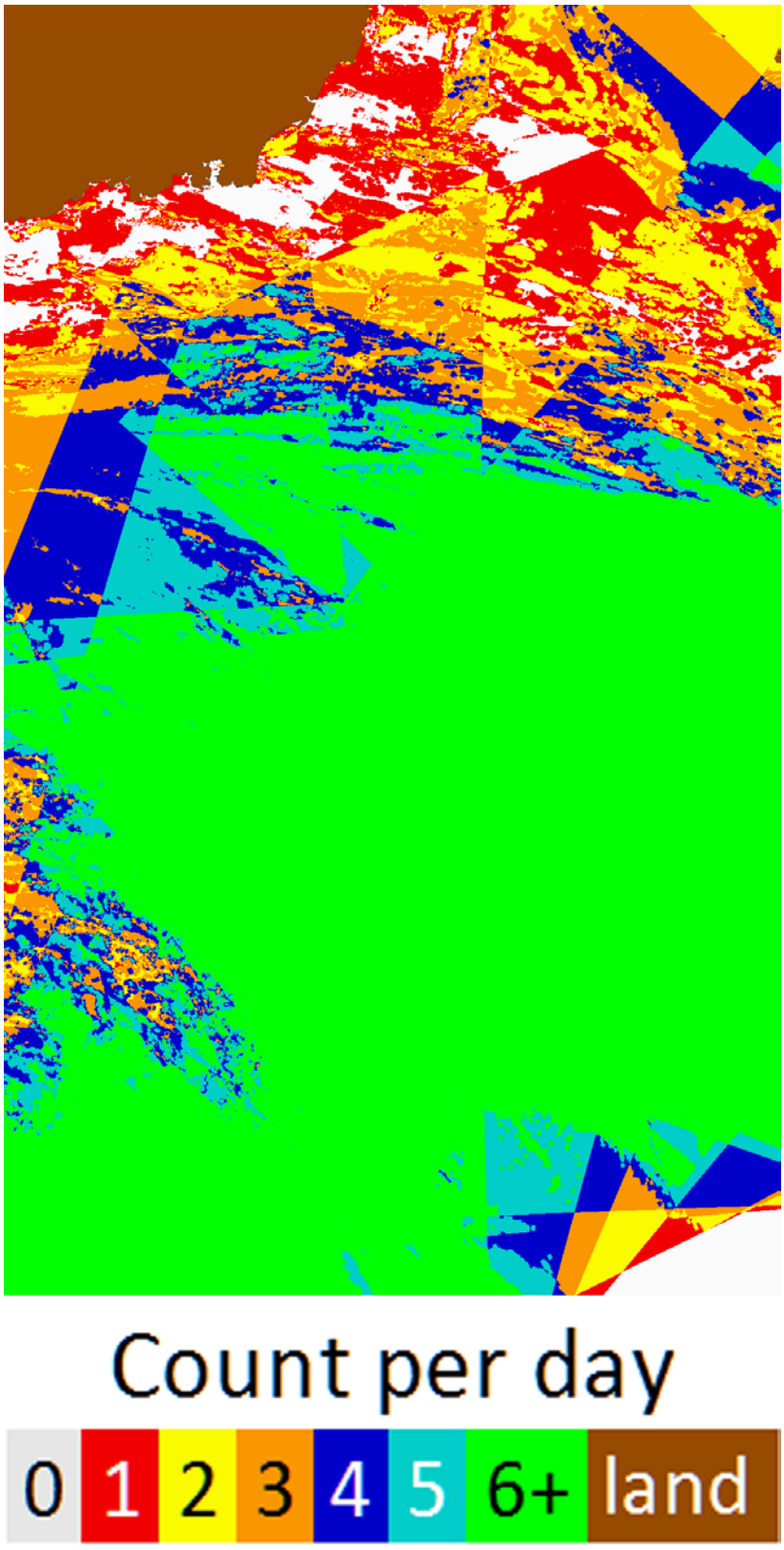

Figure 8: Daily composite of the number of cloud-free overpasses with a MODIS scan angle less than 30 degrees on 15 February 2018 in the Beaufort Sea.

3.8. Lead Detection

The leads detection algorithm begins by defining potential leads as any 1km^2 grid point from the daily composite mask where the thermal contrast of the 11 μm brightness temperature minus the mean brightness temperature greater 1.5 K and greater than the local window standard deviation.

3.8.1. Region Identification

The first step in the image processing utilizes the IDL label_region function. From the mask of all points where the thermal contrast is met one or more times, the IDL function assigns a unique region number for every object in the mask – where an object is defined as a group of more than two connected pixels. Once the region numbers are defined, the processing begins to loop through the image until all regions greater than 2 pixels in area have been processed (regions with only one or two points are rejected for being too small). The processing loop begins by selecting the largest remaining object, a search window is defined around the largest remaining object until the selection window is 750 by 750 km. The leads detection algorithm will process all potential leads within the selection window except for any potential leads that occur along or spanning across the boundary of the selection window (these boundary regions are ignored temporarily and will be processed in a later loop iteration). The algorithm continues to process the domain until all potential lead objects have been processed. The end result is a binary raster mask that records a processing code for each location and a text log file (described in 3.7.4.2).

3.8.2. Sobel Filter

For each selection window, the leads algorithm performs the following steps. First, a Sobel (1970) image filter is applied to the mask of the potential leads. This image filter helps to identify and connect linear features that might not be continuous in the native mask. This helps identify leads that may have sub-resolution elements along their path. The label_region function is used again, this time to define unique region numbers for each connected object in the Sobel filter mask. The processing logic starts with the largest Sobel filter mask region object and continues until all objects have been processed.

3.8.3. Preliminary Shape Tests

To improve processing speed, some preliminary tests are executed to exclude some objects based on shape. These tests are done because the Hough Transform (described in section 3.8.4) is computationally expensive, so some quick tests are used to reduce the number of times the Hough Transform is called.

3.8.3.1. Cloud Test

The first test excludes regions with too few repeat detections of a potential lead within the day; if more than 90% of the potential lead object area was observed two or fewer times within a day, the region is flagged (code 55) and no further processing is done. This test removes features that are most likely cloud contaminated (cloud cover may have limited the number of clear observations or else the cloud mask may have omission errors in a small number of overpasses that may result in artificially higher thermal contrast due to cloud contamination).

3.8.3.2. Width Test

Next, a test is run to test the approximate width of the region. The region area must be greater than 3 pixels (or else it will fail to have a valid line segment); the length of the diagonal line that connects the opposing corners of a rectangle that encompass the region divides the object area. Any region with an approximate width of greater than 60 km is flagged (code 62) as a non-lead feature.

3.8.3.3. Sub-region Tests

If a potential lead has passed the preliminary screening, then all remaining objects with an area greater than 3 points are subjected to more testing. First, the original mask is compared against the Sobel filtered mask to count the number of disconnected objects in the original mask that correspond to the single potential lead object region from the Sobel filter. A code non-lead flag (code 50) is assigned if an object has more than 1 sub-region, more than half of the object area is made up of sub-regions of less than 5 km^2, and there are less than five but more than two large (area greater than or equal to 5 km^2) sub-regions.

3.8.3.3.1. Symmetric Test

After testing for too many disconnected sub-regions, the next step tests the object symmetry. To do this, a box is defined around the potential lead object and if the object area in each of the four quadrants is within +/-5% of 25% then the object is classified (code 51) as too symmetric and therefore not a lead.

3.8.3.3.2. Radial Test

Similarly, if too much of an object area falls within a circle drawn over the object, it is rejected as being too circular. The circle is defined at the center of the object with a radius of half of the distance spanned in the x and y directions. And, if more than half of the object points are within 1.5km of the edge of the circle, then the object is too circular and rejected (code 52).

3.8.4. Hough Transform

If a potential lead object has passed the preliminary shape tests described in section 3.8.3, the next test is to apply a Hough Transform (Billard, 1981) to identify the longest linear feature within the region of interest.

3.8.4.1. Short Hough Line

If the Hough line has less than or equal to 3 points the region is classified as a non-lead (code 53) because the Hough line is too short.

3.8.4.2. Hough Line Region

If the Hough line is longer than 3 points, then calculate the length of the longest continuous line segment from the subset of points common between the Hough line and potential lead region. Then, define a region from the longest line segment find all of the potential lead points that are connected continuously with the line segment. This newly defined region is the sub-region that will be tested as the potential lead region. Calculate the area and length of the longest line segment within the sub-region – as it may be longer than the length the Hough line segment. If the sub-region area is greater than 2 points, a few final tests are run to classify the region as a lead or non-lead. First, a lead code (code 100) is assigned to the output mask to all points that have made it this far in the processing. Some final tests are only applied that could potentially change the mask code. Processing is done to only the largest remaining lead sub-region and regardless of the outcome of the tests, the rest of the potential lead object is processed until no more valid Hough line segment regions are found. After all of the tests described in this section, the results are written to a log file for decoding purposes. The output includes an identifier for the region number and the sub-region number, the start and end x and y coordinates as well as the latitude and longitude, the great circle object length, width, area, Hough line segment length, and the processing code. The text product for users will be generated in the characterization process described in section 3.9.

3.8.4.2.1. Segment Width Test

There is a set of two criteria to reject a sub-region of a potential lead as being too wide. First, is the width test – or region area defined in section 3.8.4.2 divided by length – is greater than 25 km^2. And second, if the ratio of sub-region area divided by the product of the span in the x multiplied by the span in the y direction is greater 1/5. If both conditions are true, the sub-region is flagged (code 61) as being too wide.

3.8.4.2.2. Segment Cloud Test

Similar the test in section 3.8.3.1, a cloud test is performed on the Hough line segment object. If more than 90% of the sub-region area was detected in less than or equal to two overpasses, then the sub-region is flagged (code 55) and rejected as a lead.

3.8.4.2.3. Segment Length and Width Test

Another test is used where the great circle length is calculated for the start and end point of the sub-region. The distance divided by the sub-region width (as calculated by area divided by length), and if the length to width ratio is less than 2, the region is flagged (code 101) as a lead with poor confidence.

3.8.4.2.4. Segment Area

The last test flags (code 56) all sub-regions with an area less than 5 km^2 as being too small. The reason the threshold is set to 5 km^2 for this test and 2 km^2 at the test in section 3.8.4.2 is so that the leads rejected for being too small (between 5 km^2 and 2 km^2) will be recorded in a processing log text file; the regions smaller than 2km^2 are not recorded in the log.

3.9. Lead Characterization

A second processing loop is used for lead characterization. The input for this processing is the mask that was described in section 3.8.1. The final product will be a raster mask described in section 4.1 and a text product described in section 4.2.

3.9.1. Region Identification

As in the lead detection process, the label_region function is used to identify and number each region where the detection technique identified a good quality lead (code 100). An erode function is applied to the label mask so that the every 1 km^2 pixel on the edge of each region is removed. The result is a mask that has more disconnected regions than the original mask; these regions are lead branch segments. Each of these smaller branch regions are numbered (via the label_region function) and then via the dilate function the regions are grown back their original size. The branches are processed in a loop.

3.9.2. Lead Branch Processing

The branch processing loop process starts by identifying the remaining branch with the largest area. Similar to the lead identification loop, the characterization loop uses a window centered around the largest remaining lead branch object. If the ratio of branch area divided by length is greater than 60 km^2 then the window is the size of the lead branch, otherwise a 750 km by 750 km window that is centered on the largest remaining lead branch is used. For each processing window, there is a loop to processes each branch (except lead branches that are on the boundary of a search window – they are processed in a window when they are not on the boundary).

3.9.2.1. Lead Branch Edge Calculations

For each lead branch, the edge of the region is defined by applying the erode function to remove the edge from the region, and then subtracting the eroded mask from the original mask. The start and end point of the lead branch is found by finding the set of coordinates that are the furthest distance apart. The great circle distance and azimuth angle are calculated from the start and end points. Dividing the segment area by great circle length derives the segment width. The region code for start and end points of the branch is recorded to more readily locate leads as a function of region – while noting that some leads may span across region boundaries.

3.9.2.2. Lead Branch Output

After all of the calculations described in section 3.9.2.1, the results are written to an ASCII file. The file contains a count variable to identify each branch, the start and end coordinates (x, y, longitude, and latitude), length, azimuth, width area, and the region code that corresponds to the start and end point of the branch. Note that lead branches that are only 1km^2 do not have a valid azimuth angle because these are points instead of line segments.

4. Leads Products

The final leads products consist of a raster image showing the location of each processed lead and a text product describing the location of each lead segment.

4.1. Raster Product Description

The derivation of the raster product output is described in section 3.8.4.2. The mask has 1 km resolution and contains the codes described in Table 1.

Mask code	Mask Color [R,G,B]	Description
10	230,230,230	Thermal contrast threshold not met
50	125,0,125	Too many disconnected sub regions
51	0,0,125	Too symmetric
52	0,125,0	Too radial
53	250,0,250	No good Hough line
55	166,166,166	Cloudy
56	255,128,0	Too small
61	0,255,0	Too wide
62	255,0,0	Preliminary width too wide
100	255,255,255	Lead
101	255,255,0	Low confidence lead; too wide for length
	150,75,0	Land

Table 1: Mask code description.

4.1.1. Raster Product Examples

An example of a raster product image is shown below in Figure 9. Refer to Table 1 for the color code for each mask color.

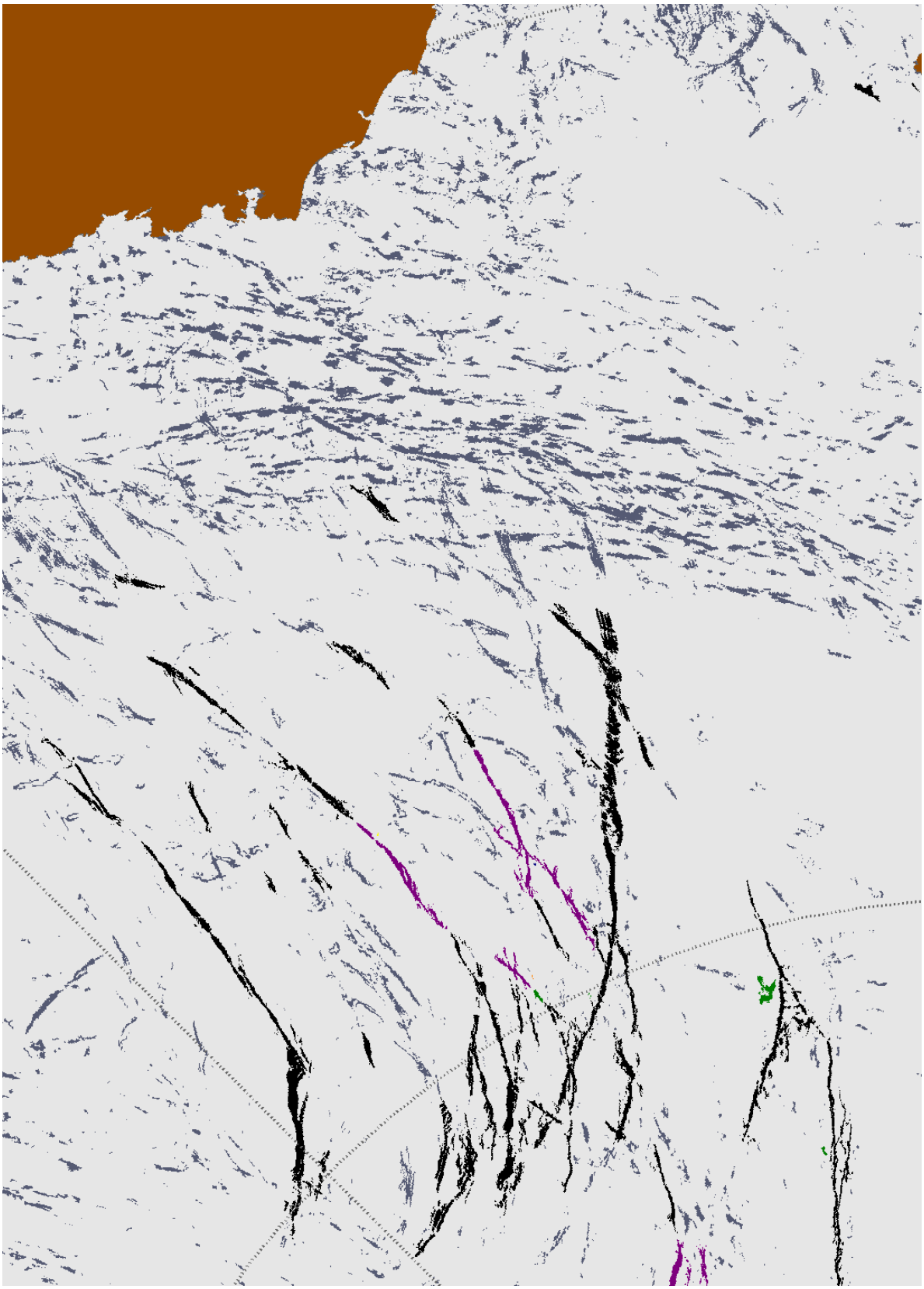

Figure 9: Leads results from 15 February 2018 in the Beaufort Sea. Accepted leads are black.

4.2. Text Product Description

The derivation of the text product is described in section 3.9.2.2.

4.2.1. Text Product Examples

An example of text product image is shown below in Table 1. Refer to section 3.9.2.2 for a description of the fields. For brevity only the first 20 (out of 18703) leads are shown.

count	x_{start}	y_{start}	x_{end}	y_{end}	lon_{start}	lat_{start}	lon_{end}	lat_{end}	length	azimuth	width	area	$region_{start}$	$region_{end}$
1	2694	4284	2677	4454	-46.621	79.916	-41.522	78.710	170.50	139.38	10.06	1716	3	3
2	2938	4340	2943	4403	-34.692	80.969	-32.525	80.522	63.05	140.97	8.66	546	3	3
3	2953	4088	2961	4152	-44.091	82.809	-40.679	82.433	64.27	128.92	5.96	383	3	3
4	2927	4275	2946	4311	-37.436	81.382	-35.272	81.223	40.50	114.89	8.99	364	3	3
5	2895	4288	2889	4322	-38.448	81.114	-37.526	80.840	34.48	151.72	8.06	278	3	3
6	2931	4447	2919	4483	-31.821	80.130	-31.378	79.798	37.96	166.72	5.19	197	3	3
7	2575	4596	2555	4614	-40.812	77.142	-40.944	76.901	27.00	7.11	6.59	178	1	1
8	2895	4399	2894	4434	-34.786	80.313	-33.797	80.048	34.96	147.05	4.92	172	3	3
9	2779	4423	2772	4452	-38.786	79.515	-38.177	79.272	29.82	154.98	5.67	169	3	3
10	2608	4547	2593	4571	-41.106	77.671	-40.923	77.419	28.38	171.01	5.92	168	1	1
11	3018	4396	3009	4420	-29.159	80.922	-28.947	80.694	25.63	171.45	6.09	156	3	3
12	2547	4626	2534	4650	-40.873	76.772	-40.649	76.532	27.39	167.74	5.44	149	1	1
13	2587	4577	2582	4591	-40.947	77.342	-40.730	77.218	14.89	158.95	8.80	131	1	1
14	2912	4504	2900	4520	-31.133	79.603	-31.230	79.425	20.02	5.69	6.24	125	3	3
15	3001	4380	3008	4404	-30.447	80.970	-29.429	80.815	24.92	133.49	4.98	124	3	3
16	2977	4333	2985	4351	-33.050	81.216	-32.094	81.118	19.61	123.15	6.12	120	3	3
17	2920	4353	2917	4377	-35.104	80.780	-34.485	80.588	24.16	152.18	4.93	119	3	3
18	2852	4230	2858	4249	-42.548	81.259	-41.544	81.168	19.83	120.08	5.80	115	3	3
19	2825	4043	2834	4064	-52.252	82.221	-50.803	82.166	22.73	104.63	3.96	90	3	3
20	2669	4465	2658	4480	-41.463	78.588	-41.388	78.421	18.64	174.84	4.51	84	3	3

Table 2: Example text product, the first 20 leads from 15 February 2018.

5. Assumptions and Limitations

The algorithm does not perform well along the edge of the sea ice; it is hard to draw the distinction between a lead and open water. Using a threshold of an 11 μm brightness temperature of 271K and below will result in the omission of leads with warm water. This is done to minimize the amount of contamination from warm clouds and maximize the detection of leads with sub-resolution ice. This threshold will be re-evaluated in future work using the 375m resolution I-band on VIIRS.

Clouds limit detection of leads. Thermal contrast is not calculated when the cloud mask identifies a cloud. The cloud mask is known to have lower accuracy in polar regions (e.g. Liu et al., 2004; Ackerman et al., 2008). Cloud and cloud shadows that are not identified by the cloud mask can be misidentified as open water and cause false lead detections. Similarly, open water features can be misidentified as clouds by the cloud mask and are thereby omitted from lead detection. Additionally, leads trends may be difficult to identify due to clouds. Cloud development may be enhanced due to the formation of leads (giving the atmosphere a source of moisture and lift – due to the water being warmer than the neighboring ice and air). And so if cloud coverage is increasing, it may be that leads are becoming more frequent, but the cloud coverage would make leads more difficult to detect (due to decreased number of clear overpasses).

This leads detection technique does not take into account ice thickness. The product does not predict where leads may likely develop nor where leads may have previously existed. Similarly, the algorithm does not make an attempt to track leads for either persistence or movement.

6. References

Ackerman, S. A., K. I. Strabala, W. P. Menzel, R. A. Frey, C. C. Moeller, and L. E. Gumley, 1998: Discriminating Clear-sky from Clouds with MODIS, *J. Geo. Res.*, **103**, D24, p. 32,141.

Ackerman, S. A., R. E. Holz, R. Frey, E. W. Eloranta, B. Maddux, and M. McGill, 2008: Cloud Detection with MODIS: Part II Validation, *J. Atmos. Oceanic Tech.*, **25**, 1073-1086.

Alam, A. and J. Curry, 1995: Lead-induced atmospheric circulations. *J. Geophys. Res.*, **100**, C3, 4643-4651.

Appel I., and J. A. Kenneth, 2002: Fresh water ice Visible/Infrared Imager/Radiometer Suite algorithm theoretical basis document, Version 5. SBRS document #: Y2404.

Ballard, D. H., 1981: Generalizing the Hough Transform to Detect Arbitrary Shapes, Pattern Recognition, Vol. 13, No. 2, p. 111-122.

Frey, R. A., S. A. Ackerman, Y. Liu, K. I. Strabala, H. Zhang, J. Key and X. Wang, 2008: Cloud Detection with MODIS, Part I: Recent Improvements in the MODIS Cloud Mask, *JTECH* **25**, 1057-1072.

Fraser, A. D., R. A. Massom, 2009: A Method for Compositing Polar MODIS Satellite Images to Remove Cloud Cover for Landfast Sea-Ice Detection, IEEE Transactions on Geoscience and Remote Sensing, Vol. 47, No. 9, 3272-3282.

Hakkinen, S., A. Proshutinsky, and I. Ashik, 2008: Sea ice drift in the Arctic since the 1950s, *Geophys. Res. Lett.*, **35**, L19704, doi:10.1029/2008GL034791, 184.

Hall D.K., G.A. Riggs, and V.V. Salomonson, 2001: Algorithm theoretical basis document for the MODIS snow and sea ice mapping algorithms.

Hall D.K., G.A. Riggs, and V.V. Salomonson, 2006: MODIS sea ice products user guide to collection 5.

Hall D.K., G.A. Riggs, and V.V. Salomonson, 2015: MODIS sea ice products user guide to collection 6. Available online http://nsidc.org/data/docs/daac/modis/pdf/modis-sea-ice-user-guide-C6.pdf.

Key, J, 1994: The area coverage of geophysical fields as a function of sensor field-of-view. *Remote Sensing Environ*., 48(3), 339-346.

Key, J., J.A. Maslanik, and E. Ellefsen, 1994: The effects of sensor field-of-view on the geometrical characteristics of sea ice leads and implications for large-area heat flux estimates. *Remote Sensing Environ*., **48**(3), 347-357.

Key, J., R. Stone, J. Maslanik, and E. Ellefsen, 1993: The detectability of sea ice leads in satellite data as a function of atmospheric conditions and measurement scale. *Annals Glaciol*., **17**, 227-232.

Key, J. and M. Haefliger, 1992: Arctic ice surface-temperature retrieval from AVHRR thermal channels. *J. Geophys. Res.-Atmospheres*, *97*, 5885-5893.

Key, J.R.; J.B. Collins, C. Fowler, and R.S. Stone, 1997: High-latitude surface temperature estimates from thermal satellite data. *Remote Sensing Environ.*, *61*, 302-309.

Liu, Y.; J. Key, and R. Mahoney, 2016: Sea and freshwater ice concentration from VIIRS on Suomi NPP and the future JPSS satellites, *Remote Sens.*, *8*, 523.

Liu Y., and J.R. Key, 2010: Algorithm theoretical basis document for ABI ice cover and concentration. NOAA NESDIS center for satellite applications and research.

Liu Y., J.R. Key, R. A. Frey, S. A. Ackerman, and W. P. Menzel, 2004: Nighttime polar cloud detection with MODIS. Remote Sens. Environ., 92, 181–194, doi:10.1016/j.rse.2004.06.004.

Maykut, G. A., 1978: Energy exchange over young sea ice in the central Arctic. *J. Geophys. Res*., **83** (C7), 3646-3658.

Miles, M. W., and R. G. Barry, 1998: A 5-year satellite climatology of winter sea ice leads in the western *Arctic, J. Geophys. Res*., **103**(C10), 21,723–21,734, doi:10.1029/98JC01997.

Murray, R.J., and I. Simmonds, 1995: Responses of climate and cyclones to reductions in Arctic winter sea ice. *J. Geophys. Res*., **100**, 4791-4806.

Smith, S. D., R. D. Muench and C. H. Pease, 1990: Polynyas and leads: An overview of physical processes and environment, J*. Geophys. Res*. **95**, 9461-9470.

Sobel, I. "Camera Models and Perception," Ph.D. thesis, Stanford University, Stanford, CA, 1970.

Stone, R. and J. Key, 1993. The detectability of winter sea ice leads in thermal satellite data under varying atmospheric conditions, *J. Geophys. Res*., 98(C7), 12469-12482.

Willmes, S. and G. Heinemann, 2015: Pan-Arctic lead detection from MODIS thermal infrared imagery. *Annals of Glaciology*, 56, 29-37.

Zwally, J., et al., 2002: ICESat's laser measurements of polar ice, atmosphere, ocean and land, *J. Geodyn*., **34**, 405–445.